Visually Guided Needle Driving and Pull for Autonomous Suturing

Orhan Özgüner, Tom Shkurti, Su Lu, Wyatt Newman, and M. Cenk Çavuşoğlu

Abstract—This paper presents a visually-guided autonomous needle driving algorithm for autonomous robotic surgical suturing. Surgical needle tracking, needle path planning, and optimum needle grasp selection algorithms are employed. The procedure is performed in 5 major steps: needle grasp, needle hand-off, needle drive, needle regrasp, and needle pull. The performance of the procedure is experimentally evaluated using the physical da Vinci® surgical robotic system and da Vinci Research Kit (dVRK). Initial results suggest that the dVRK can successfully perform needle driving with visual guidance.

I. INTRODUCTION

While fully autonomous surgery will be a challenge in the near future, autonomous robotic surgical assistants [1] have been proposed to perform low-level manipulation tasks such as suturing [2]-[4], debridement [5], dissection [6], resection [7], needle grasping [8], [9], suture planning [2], [10], [11], and retraction [12] to enhance surgeon performance and reduce operation time. Due to its repetitive nature, suturing is ideally suited to this form of automation. To reduce the tissue trauma and operation time, an automation framework can keep the surgeon as the decision maker while relying on the robotic system to manage the execution of low-level motions. As opposed to the use of primarily pre-planned manipulation strategies employed in traditional industrial robotics applications, the dynamic nature of surgical environments and the underlying substantial uncertainty necessitates that surgical manipulations to be performed under sensory guidance. As such, methods for perceiving the state of the surgical environment and the robotic system are a key requirement for autonomous and semi-autonomous execution of surgical manipulation tasks [13]-[16]. Once such robust robotic perception algorithms are available, they can be used to perform precise visually-guided manipulations, allowing the robotic surgical system to operate under imperfect and varying robotic manipulator/camera-calibration conditions, and to deal with the uncertainties resulting from unknown initial conditions and complex tissue deformation dynamics.

This study specifically focuses on visually-guided surgical needle driving for autonomous suturing tasks in RMIS. The steps of the procedure are determined using the best practices of manual suturing with a semi-circular needle. The proposed method uses tools available in a regular RMIS operation without modifying them. The task-critical element, the surgical needle, is localized and tracked during the entire

This work was supported in part by the National Science Foundation under grants CISE IIS-1524363, CISE IIS-1563805, and DUE-1928485.

The authors are with the Departments of Electrical, Systems, and Computer Engineering, and Computer and Data Sciences, Case Western Reserve University, Cleveland, OH. They can be reached via email at {oxo31,tes77,sxl924,wsn,mcc14} @case.edu respectively.

task and its 3D position and orientation is provided to the other components of the algorithm.

In the presented method, the suturing task starts with one of the robotic surgical manipulators grasping the surgical needle, which is randomly placed within the workspace observable through the endoscope. Then the robot hands over the needle to the other robotic surgical manipulator to provide a better needle grasp configuration for the needle drive. Human surgeons perform this step frequently in RMIS since the grasp configuration directly affects the quality of the suture. The robotic manipulator then drives the needle through the tissue. Once the tip of the needle exits the tissue, the robot releases the base of the needle and regrasps the needle from the tip using visual information from the tracking algorithm. The visually-guided needle driving is completed by pulling the needle out of the tissue. Several repetitions of these steps form a running suture.

This study performs a fully autonomous needle drive and pull without using any aid such as a painted needle, pregrasped needle, angle positioning end-effector apparatus for needle grasping, external stereo camera system, or human intervention. Unlike prior literature, in the proposed approach the needle is randomly placed in the workspace, then picked up and handed over from one manipulator to the other, with only visual guidance. The hand-off is particularly demanding since it requires precise needle positioning. Additionally, most previous methods do not release the needle freely in the tissue, whereas the approach presented in this study has the capability to release the needle in the tissue and regrasp it using visual guidance to pull it out.

This paper builds on prior work in needle path planning [2], needle tracking [15], optimum needle grasp selection [8], and surgical robot-camera calibration [17].

The paper is organized as follows: Section II discusses related studies. In Section III, the problem definition and the proposed methods are introduced. The specific details of hardware based validation tests and the results of the visually-guided needle driving are presented in Section IV. The conclusions are presented in Section V.

II. RELATED STUDIES

One of the major steps of the autonomous suturing task is driving the needle through the tissue. Once the needle is inserted into and driven through the tissue by its base, it must be regrasped from the tip and pulled out again. Researchers studying the autonomous suturing task have tried to solve this problem using various methods:

Staub et al. developed an autonomous tissue piercing method for RMIS using a semi-circular needle. The incision

point is communicated to the robot using a laser pointer and needle positioning employs a visual servoing approach. The robot posture is initialized manually to hold the needle perpendicular to the jaws of the end-effector. This prior positioning minimizes the risk of a slip during the piercing process. The needle tip, which is colored, is tracked in the image frame rather than tracking the position and orientation of the needle in the world frame. This method only pierces the tissue with the needle, and needle regrasp and pull are not performed [18].

Iyer et al. attempted to solve the suturing problem by using a single-arm robotic manipulator with a standard laparoscopic needle holder, a semi-circular surgical needle and a clinical endoscope (single camera). The needle driving procedure was performed with a pregrasped needle. A monocular pose measurement method was used along with the least-square ellipse-fitting OpenCV functions to estimate the position and orientation of the semi-circular needle. The suture surface was identified using green circular stickers and the needle entry/exit points were chosen manually by the surgeon on the console [19].

Sen *et al.* developed an automated multi-throw surgical suturing algorithm using the da Vinci® surgical system. Instead of surgical endoscope images, a custom stereo camera pair was employed to provide a larger workspace and a yellow-painted surgical needle was used. The needle's distinctive shape and color were leveraged to calculate the 3D pose of the needle using an ellipse fitting algorithm. To avoid inaccurate grasping, a "Suture Needle Angular Positioner" was used to align and hold the needle in a known orientation. Additionally, the procedure started with the robot already holding the needle rather than grasping the needle from the scene [4].

Shademan *et al.* demonstrated an *in vivo* supervised autonomous soft tissue surgery using a plenoptic 3D and near-infrared fluorescent (NIRF) imaging system. A vision-guided robotic system was equipped with an actuated suturing tool which was capable of performing a running suture. The supervisory control architecture of the system allowed the surgeon to select incisions and track the placements of stitches [20]. Recently, this study was further expanded by developing a new 3D imaging endoscope, new actuated tool, and a suture planning method for the autonomous suturing task [21].

The earlier studies in the literature on autonomous needle driving methods all rely on simplifying assumptions such as artificially colored needles, a pregrasped needle, angle positioning end-effector apparatus for the needle grasping, or custom built end-effector and camera systems, none of which are applicable to practical RMIS scenarios. In contrast, the present study aims to perform fully autonomous needle driving using images from the endoscopic stereo cameras of a realistic RMIS system without any modification to the robotic tools, endoscopes, or the surgical needles. This study uses visual guidance while grasping and handing over the needle; and the tracking algorithm provides 3D position and orientation of the needle for planning. This condition requires

a robust needle tracking algorithm capable of tracking the needle under high occlusions. To the best of the authors' knowledge, there are also no earlier published studies using such a realistic system without modifications where the needle is released in the tissue and regrasped for pulling while relying only on a visual tracking system.

III. METHODS

The visually-guided needle driving task starts with the needle placed randomly on the tissue. Next the tissue surface and the suture line are visually identified. Then the needle tracking algorithm locates the needle and tracks it during the entire task, meaning that the needle pose is available at any time. The task proper then starts by grasping the surgical needle with one of the surgical manipulator arms. Next, the robot moves to an advantageous pose to hand over the needle to the other surgical manipulator. This step provides a better grasping configuration for driving the needle than could be acquired with the needle lying flat against the tissue. Once the needle is in the other surgical manipulator, the manipulator brings the needle to the suture entry point at the correct insertion orientation. When the needle tip is at the suture entry point, the robot drives the needle through the tissue by rotating the needle around the needle center to minimize the tissue tear. Once the tip of the needle exits the tissue, the manipulator releases the needle base to regrasp it from its tip. Finally, the robot regrasps the needle tip and pulls the needle out of the tissue.

A. Surface and Suture Line Identification

The incision to be sutured is represented with a 5cm dark line drawn on the light-colored suture pad. The start-and end-points of the suture are identified in image space using standard image-processing techniques: Canny edge detection [22] followed by extracting the longest line from a probabilistic Hough transform [23]. Fiducials (visible in Fig. 1 as 6 small circles) aide in identifying the 3D location of the tissue surface in the absence of sufficient texture on the suturing training pad from which the depth could be properly determined (Fig. 1).

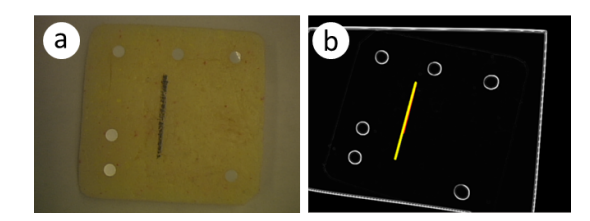


Fig. 1. (a) Endoscopic view of the phantom tissue manufactured by Simulab Corp. (b) Tissue with suture line highlighted.

B. Needle Localization and Tracking

The position and orientation of the needle are determined and tracked using the particle-filter-based algorithm described in detail in [15]. The core idea of the particle filter algorithm is to approximate the posterior probability distribution of a state, such as the surgical needle pose, by

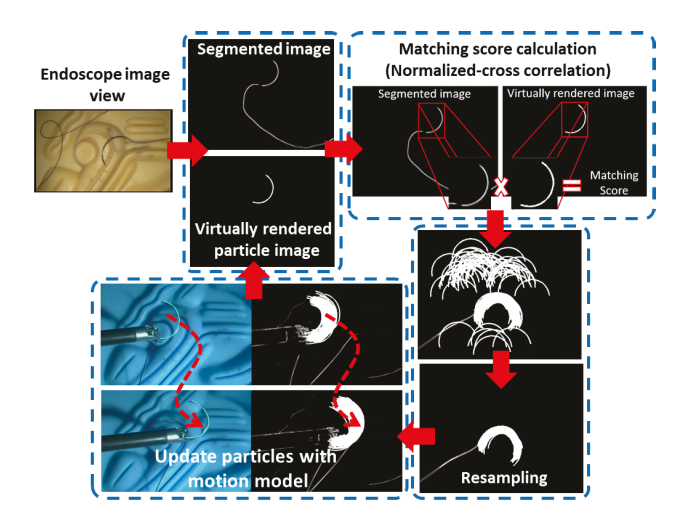


Fig. 2. Particle filter algorithm flow for needle localization and tracking.

using a finite number of randomly-generated samples, called particles. The overall flow diagram can be seen in Fig. 2.

Since the visually-guided needle driving procedure starts with placing the needle freely in the surgical scene, the initial set of particles are randomly generated in the workspace. If the rough pose of the needle is known, then this can be used to reduce the computation necessary to solve the global localization problem at the initialization stage.

The first step in the algorithm is to update the particle states using a motion model. In this study, there are two different cases for the update step. If the needle is free, i.e., not being held by the robot, then the motion of the needle is modeled as Brownian motion, where the state of each particle is perturbed at each time step with Gaussian noise. If the needle is grasped by the robot, then each particle state is updated using the incremental motion of the robotic gripper holding the needle.

For the measurement update step, the images acquired by the endoscope are segmented using a thin feature extraction algorithm [14] in order to emphasize the needle outline. The observation likelihoods are then estimated from the image-space similarity between the virtual images of the needle generated from the needle pose hypotheses, and the observed segmented images of the scene, as calculated using the normalized cross-correlation. In the final step of the algorithm, particles are resampled using the low variance resampling method [24].

The needle tracking algorithm runs as a separate Robot Operating System (ROS) node which publishes the position and orientation of the needle at all times. The steps outlined above are implemented on a GPU-based schema using the CUDA parallel computing platform. This implementation is able to run at ~ 3 frames per second with 3000 particles, which is sufficient to track the needle for the autonomous visually guided needle driving task.

C. Needle Grasp

The pose of the needle is obtained from the tracking algorithm described in Section III-B, and the initial grasp

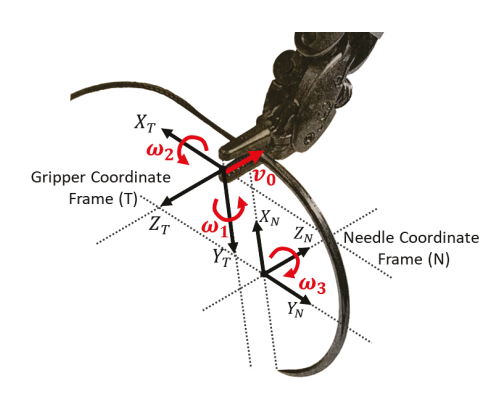


Fig. 3. Grasp configuration parameterization. The origin of the frame **T** is at the tip of the gripper. The Y axis is perpendicular to the jaw of the gripper and Z axis points points along the gripper. The origin of the frame **N** is placed at the center of the needle. The X axis points to the base of the needle and the Y axis points to the body of the needle.

is performed with the most feasible grasp as determined by [8].

Needle grasping is managed by the ROS *MoveIt!* package, which provides built-in trajectory planning and kinematics functionality to grasp arbitrary objects using arbitrary manipulators defined based on a robot kinematic description, an object model, and a user-determined grasp transform G_{TN} .

The grasp configuration of the surgical needle is parameterized with 4 DoFs as shown in Fig. 3. The gripper coordinate frame **T** is placed on the tip of the gripper. Its Y axis is perpendicular to the jaw of the gripper and its Z axis points along the gripper. The needle coordinate frame **N** is placed at the center of the needle. Its X axis points to the base of the needle and its Y axis points to the body of the needle. The kinematics of the grasp configuration is parameterized by one translation and three rotations. As can be seen from the Fig. 3, ϑ_0 specifies the insertion translation along the negative Z axis of the **T** frame. ω_1 and ω_2 are defined around axes passing through the origin of the gripper frame, and ω_3 is defined to be around an axis passing through the center of the needle [8].

A full 4×4 grasp transformation matrix between frame **T** and frame **N** can be computed from these parameters as follows, where r is the radius of the needle, $s_i = sin(\theta_i)$, and $c_i = cos(\theta_i)$:

$$R = \begin{bmatrix} s_1 s_3 - c_1 c_3 s_2 & -c_1 c_2 & -c_3 s_1 - c_1 s_2 s_3 \\ -c_1 s_3 - c_3 s_1 s_2 & -c_2 s_1 & c_1 c_3 - s_1 s_2 s_3 \\ -c_2 c_3 & s_2 & -c_2 s_3 \end{bmatrix}$$

$$p = \begin{bmatrix} r(c_1 s_2 (c_3 - 1) - s_1 s_3) - \theta_0 \\ r(c_1 s_3 + s_1 s_2 (c_3 - 1)) \\ rc_2 (c_3 - 1) \end{bmatrix}$$

$$G_{TN}(\theta_0) = \begin{bmatrix} R(\theta_0) & p(\theta_0) \\ 0 & 0 & 0 & 1 \end{bmatrix}$$

$$(1)$$

The needle grasping method is implemented in an actionserver schema which takes a goal state consisting of the

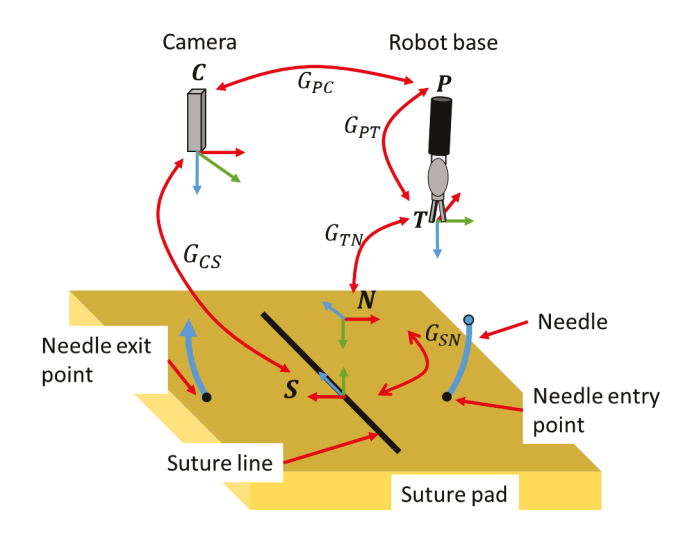


Fig. 4. The origin of the frame \mathbf{T} is at the tip of the gripper, \mathbf{N} is at the center of the needle, \mathbf{S} is on the suture line, \mathbf{P} is at the RCM of the manipulator, and \mathbf{C} is at the camera. G_{PT} is the transform between the robot base (\mathbf{P}) and the gripper (\mathbf{T}) frames, G_{PC} is the hand-eye calibration, G_{CS} is the transform between the camera (\mathbf{C}) and the tissue frames (\mathbf{S}), and G_{TN} is the transform between the gripper and the needle.

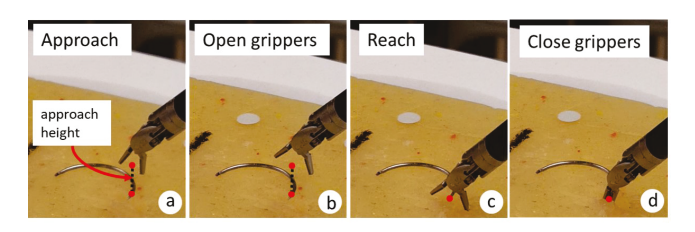


Fig. 5. *MoveIt!* also divides the needle hand-off motion into approach, reach, and grasp steps. The manipulator begins aligned with the needle orientation, then approaches the needle position to a user defined offset along the z-axis of the manipulator (a), opens its grippers (b), reaches the non-offset pose of the needle (c), and closes the grippers(d).

desired grasp transform (defined by the 4 parameters described above) and the manipulator arm (identified by ID number) with which to perform the grasp. The action server obtains the most recent needle pose published by the needle tracking algorithm and calls the *MoveIt!* package to plan a motion which will end at the goal state. *MoveIt!* plans the grasping motion in three steps: approach, reach, and grasp. In the approach step, the manipulator moves to the needle pose with a user-defined offset along the z-axis of the end-effector. Then, the manipulator opens the grippers and reaches to the actual goal grasp configuration. The needle grasp is then finalized by closing the grippers (Fig. 5).

D. Needle Hand-off

As described in [8], the grasp configuration of the needle directly impacts the suture quality and success rate. In order to obtain a good grasp, surgeons often change the needle configuration by passing it from one manipulator to another. Therefore, this study employs an automated handoff step to obtain an optimal needle grasp transform. The handoff procedure has three steps. Once the needle is grasped by first manipulator using the grasping method described in Sec. III-

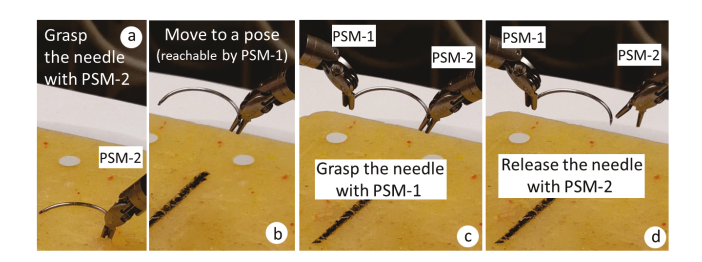


Fig. 6. Needle handoff steps. The needle is grasped by one of the manipulators (a). The manipulator then moves to a pose within the camera view where it is reachable by the other manipulator (b). Needle grasping is performed using the other manipulator(c). Then the first manipulator releases the needle and moves away without disturbing the grasp configuration (d).

C, the manipulator moves to a pose under the camera view where the needle is more easily reachable by the second manipulator. At this position, the second manipulator grasps the needle using the procedure described in Sec. III-C, which uses an optimal grasp configuration (selected as described in detail in [8]). Finally, first manipulator releases the needle and moves away without disturbing the grasp configuration (Fig. 6).

E. Needle Drive

In the needle driving phase, the needle trajectory is calculated using the needle path planning algorithm as described in detail in [2]. For the purpose of trajectory planning, the tissue surface is assumed to be a plane and the needle is approximated as a semicircle with a known radius. In addition to these constants, the depth of the suture (d) is defined by the surgeon. The needle entry point (g) and the exit point (f) can be computed using the suture depth (d) and the needle radius (r) (Fig. 7). Using the available geometry, the transform between local frames of the needle (N) and the tissue (S), G_{SN} , can be calculated as follows:

$$G_{SN}^{\alpha} = \begin{bmatrix} & & & 0 \\ & R_Z(\alpha) & & h \\ & & & 0 \\ 0 & 0 & 0 & 1 \end{bmatrix}.$$
 (2)

Then the end-effector trajectory can be computed as:

$$G_{PT} = G_{PC} \cdot G_{CS} \cdot G_{SN}^{\alpha} \cdot G_{TN}^{-1}, \tag{3}$$

where G_{PT} is the transform between the robot base (**P**) and the end-effector (**T**) frames, G_{PC} is the hand-eye calibration, G_{CS} is the transform between the camera (**C**) and the tissue frames (**S**), and G_{TN} is the transform between the end-effector and the needle (Fig. 4). The rotation angle α ranges from α_0 to $\pi - \alpha_0$, increasing incrementally as the drive progresses, and α_0 can be computed as:

$$\alpha_0 = \arcsin(h/r),$$

$$\alpha_0 \le \alpha \le \pi - \alpha_0,$$
(4)

where h=r-d is the height of the needle center C from the tissue surface (Fig. 7). Once the tool tip trajectory is obtained, the robot executes the needle drive. First the manipulator approaches the needle entry point along with the

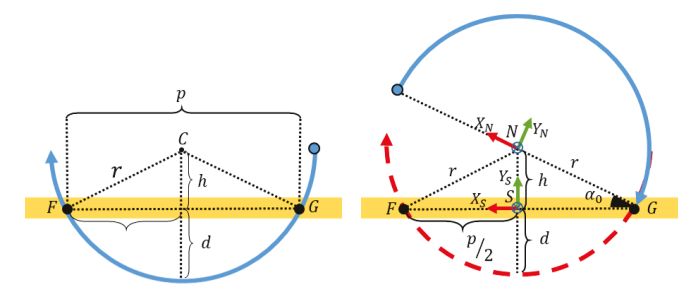


Fig. 7. The depth of the needle in the tissue (d) is specified by the surgeon. The needle entry point G, exit point F, and the height of the needle center C(h) are determined from needle radius F and F as shown on the left. The transformation between the needle F and the tissue F frames F can then be computed. Once the needle penetrates the tissue, it is possible to rotate the needle so that it will naturally drive to the exit point, as shown on the right. The dashed view of the needle is the end position of the needle after a successful drive.

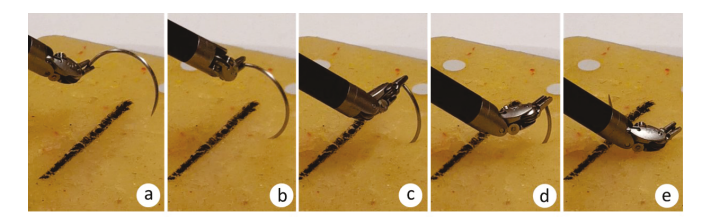


Fig. 8. Image sequence from the needle driving task. (a) The manipulator first moves the needle tip to the suture entry point, approaching along the z-axis of the end-effector. (b) Once it reaches the desired entry point, it rotates around the needle center point while minimizing the stress on the entry point (c-e).

z-axis of the manipulator and then rotates around the center of the needle to insert it into the tissue. Fig. 8 shows an image sequence of the needle drive trajectory execution. After successfully driving the needle, the manipulator releases the needle base to regrasp it from the tip.

F. Needle Regrasp and Pull

Once the needle reorientation is completed, the needle pull phase starts. In order to follow through with the suture, the needle is first regrasped by the manipulator using the needle grasp method described in Section III-C. The needle pose information needed to determine the manipulator pose for regrasping the needle is obtained from the needle tracking algorithm (Section III-B). Once the needle tip is grasped, the manipulator moves the needle out of the tissue while minimizing the tissue deformation by moving the needle along its own arc (Fig. 9) similar to the needle drive phase.

IV. EXPERIMENTS AND RESULTS

A. Hardware description

In order to control the da Vinci[®] surgical robotic system in an automated manner, the open-source/open-hardware da Vinci Research Kit (dVRK) [25] is employed (Fig. 10). The dVRK acts as a substitute for the teleoperation master station via a ROS interface that can be controlled from any desktop computer. Forward and inverse kinematics allow this joint-level control to be leveraged into workspace (3D cartesian) control of the robot in the manipulator (PSM) base frame.

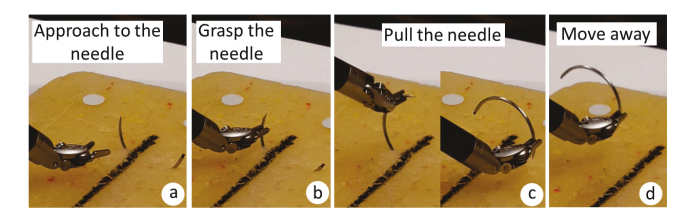


Fig. 9. Needle regrasp and pull phase steps. The manipulator approaches the needle (a). Then the manipulator grasps the needle (b). The needle is pulled out of the tissue along its own arc (c). The manipulator moves away to finish the needle driving task (d).

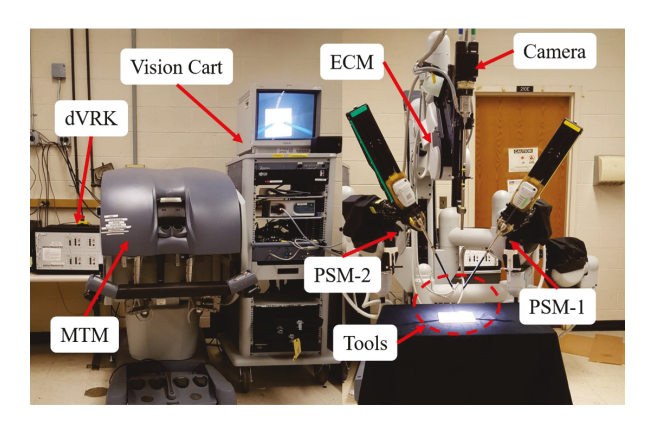


Fig. 10. daVinci® surgical robotic system with the daVinci Research Kit.

Multiple manipulators can be managed in parallel by the device.

B. Experiments

The experimental validation of the visually guided needle driving procedure is presented in this section. To test the needle drive, a surgical suture needle was driven through a tissue phantom using a da Vinci[®] IS-1200 Surgical Robotic System, upgraded with the dVRK [25]. A 26 mm diameter semi-circular taper point CT-1 surgical needle manufactured by Ethicon Inc. was used for the experiments. The phantom tissue was an SCS-10 subcuticular tissue simulator manufactured by Simulab Corp. as a surgical training aid. This homogeneous phantom tissue produces repeatable results that depend on the type of needle drive and not the location of the suture. In addition, the phantom tissue deforms when the needle is inserted to introduce uncertainty.

The needle driving experiments were performed using the methods described in Section III. All of the experiments were conducted autonomously without any human intervention. The visually-guided needle drive method was broken into five steps: Needle Grasp (NG), Needle Hand-Off (NH), Needle Drive (ND), Needle Regrasp (NR), and Needle Pull (NP). The result of each step is recorded as success or fail. If the robot failed on a step, any subsequent step was recorded as a fail.

An approximately 5cm straight line was drawn on the phantom tissue using a black ink marker to simulate the incision that will be sutured. The needle and the tissue were placed randomly within the camera view (provided that the needle was reachable by the robot end effector). The system was then initialized with a desired suture depth (d), needle diameter (r), and approach distance for needle grasping. A total of 20 visually-guided needle driving trials were performed and results were recorded. The results of each trial can be found in Table I and detailed success rates in Table II.

C. Results

Table I shows the detail of the success/failures in each step of each of the trials. Out of 20 trials, the robot successfully performed the operation in 14 cases (70%). Specifically, the robot successfully grasped the needle in 19 cases (95%), successfully handed over the needle in 18 cases (90%), successfully drove the needle in 18 cases (90%), regrasped the needle in 14 cases (70%), and pulled the needle out in 14 cases (70%).

Since the result of each step of the procedure affected the result of its successor, the success rate of a step excluding failures due to the earlier steps is additionally calculated in Table II. The individual results of each step of the task are as follows: The robot successfully grasped the needle in 19/20 cases (95%). The failure to grasp the needle occurred because the needle localization algorithm estimated the needle closer to the camera than it actually was. The robot successfully handed over the needle in 18/19 cases (94.7%). In the failure case, the robot missed the needle because the needle tracking algorithm estimated the needle to be further away from the camera than it actually was. The needle was successfully driven in 18/18 cases (100%). Once the robot grasped the needle, it could always drive the needle trough the tissue. The robot regrasped the needle in 14/18 cases (77.7%). In all 4 failure cases, the robot missed the needle because of X-Y tracking inaccuracy. The robot then successfully performed the needle pull in 14/14 (100%) cases. Once the robot regrasped the needle, it could always successfully pull the needle out of the tissue. The video attachment contains several successful visually guided needle drives as well as the failure cases.

V. CONCLUSIONS

This study presents an automated visually-guided needledriving method for autonomous suturing. This work builds on needle path planning, needle tracking, and optimum needle grasp selection algorithms developed in our earlier work. In the proposed approach, a needle tracking algorithm is employed to provide needle pose information throughout the task to guide the needle manipulations. The suturing pad surface and the wound locations are identified using computer vision techniques. The suture entry/exit points are then computed from this surface information. The task is then performed in 5 major steps: needle grasp, needle handoff, needle drive, needle regrasp, and needle pull. Execution of these steps performs a successful visually guided needle driving. Multiple repetitions of the procedure would form a running suture. The performance of the procedure is experimentally evaluated using the physical da Vinci®

TABLE I

RESULTS FOR NEEDLE DRIVING EXPERIMENT. 20 TRIALS WERE PERFORMED. FOR THE NEEDLE DRIVING STEPS, NG REPRESENTS INITIAL NEEDLE GRASP, NH REPRESENTS NEEDLE HAND-OFF, ND REPRESENTS NEEDLE DRIVE, "NR" REPRESENTS NEEDLE REGRASP, AND "NP" REPRESENTS NEEDLE PULL.

.	NG	2777	NID	NID	NID
Experiment	NG	NH	ND	NR	NP
1	V	~	~	~	V
2	~	~	~	~	~
3	×	×	×	×	×
4	~	~	~	~	~
5	~	×	×	×	×
6	V	~	~	~	~
7	~	~	~	~	~
8	~	V	~	×	×
9	~	~	~	~	~
10	~	/	~	~	×
11	~	~	~	*	×
12	~	~	~	~	'
13	~	~	~	~	~
14	~	~	~	~	/
15 16	\(\times \)	~	~	×	×
16	~	V	~	~	~
17	~	~	~	×	×
18	1	V	~	~	~
19	~	~	~	~	~
20	~	~	~	~	~

TABLE II

OVERALL AND INDIVIDUAL STEP SUCCESS RATES OVER THE NEEDLE DRIVING EXPERIMENT. 20 TRIALS WERE PERFORMED WITH AN OVERALL 70% SUCCESS RATE. EACH INDIVIDUAL STEP OF THE EXPERIMENT WAS AFFECTED BY PREVIOUS STEP. THEREFORE, THE INDIVIDUAL MEAN IS CALCULATED SEPARATELY WHILE EXCLUDING ANY FAILURES IN PREVIOUS STEP.

Experiment	NG	NH	ND	NR	NP
Overall Mean	95%	90%	90%	70%	70%
Individual Mean	95%	94.7%	100%	77.7%	100%

surgical robotic system. The validation results indicate that the proposed method can successfully drive a surgical needle using visual guidance, and the initial experiments in this paper confirm that the system presented can computationally plan and execute visually-guided needle driving task.

Future work will proceed in several directions. Although the tracking algorithm is implemented on a GPU-based parallel computing scheme, the frame rate (3 frames per second for 3000 particles) is currently insufficient for closed-loop visual servo control. We are therefore working on improving the speed of the tracking algorithm up to a sufficient frame rate for a closed-loop visual servo control by optimizing the GPU-based implementation. The closed-loop visual servo control will improve the success rate of the procedure. Another direction will take place in combining the presented study with previous developed suture thread tracking [14] and knot tying [3] algorithms to perform the suturing task fully autonomously.

REFERENCES

- [1] G. P. Moustris, S. C. Hiridis, K. M. Deliparaschos, and K. M.Konstantinidis, "Evolution of autonomous and semi-autonomous robotic surgical systems: a review of the literature," *The International Journal of Medical Robotics and Computer Assisted Surgery*, vol. 7, no. 4, pp. 375–392, 2011.
- [2] R. C. Jackson and M. C. Cavusoglu, "Needle path planning for autonomous robotic surgical suturing," in *IEEE International Conference on Robotics and Automation (ICRA)*, 2013.
- [3] D. Chow, R. C. Jackson, M. C. Cavusoglu, and W. Newman, "A novel vision guided knot-tying method for autonomous robotic surgery," in 2014 IEEE International Conference on Automation Science and Engineering (CASE), Aug 2014, pp. 504–508.
- [4] S. Sen, A. Garg, D. V. Gealy, S. McKinley, Y. Jen, and K. Goldberg, "Automating multi-throw multilateral surgical suturing with a mechanical needle guide and sequential convex optimization," in 2016 IEEE International Conference on Robotics and Automation (ICRA), May 2016, pp. 4178–4185.
- [5] B. Kehoe, G. Kahn, J. Mahler, J.-H. Kim, A. Lee, A. Lee, K. Naka-gawa, S. Patil, W. D. Boyd, P. Abbeel, and K. Goldberg, "Autonomous multilateral debridement with the raven surgical robot," in *IEEE International Conference on Robotics and Automation (ICRA)*, 2014.
- [6] D. Nagy, T. D. Nagy, R. Elek, I. J. Rudas, and T. Haidegger, "Ontology-based surgical subtask automation, automating blunt dissection," *Journal of Medical Robotics Research*, vol. 03, no. 03n04, p. 1841005, 2018. [Online]. Available: https://doi.org/10.1142/S2424905X18410052
- [7] J. D. Opfermann, S. Leonard, R. S. Decker, N. A. Uebele, C. E. Bayne, A. S. Joshi, and A. Krieger, "Semi-autonomous electrosurgery for tumor resection using a multi-degree of freedom electrosurgical tool and visual servoing," in 2017 IEEE/RSJ International Conference on Intelligent Robots and Systems (IROS), Sep. 2017, pp. 3653–3660.
- [8] T. Liu and M. C. Cavusoglu, "Needle grasp and entry port selection for automatic execution of suturing tasks in robotic minimally invasive surgery," *IEEE Transactions on Automation Science and Engineering*, vol. 13, no. 2, pp. 552–563, April 2016.
- [9] C. D'Ettorre, G. Dwyer, X. Du, F. Chadebecq, F. Vasconcelos, E. D. Momi, and D. Stoyanov, "Automated pick-up of suturing needles for robotic surgical assistance," *CoRR*, vol. abs/1804.03141, 2018.
- [10] S. A. Pedram, P. Ferguson, J. Ma, E. Dutson, and J. Rosen, "Autonomous suturing via surgical robot: An algorithm for optimal selection of needle diameter, shape, and path," in 2017 IEEE International Conference on Robotics and Automation (ICRA), May 2017, pp. 2391–2398.
- [11] S. A. Pedram, P. Ferguson, J. Ma, E. P. Dutson, and J. Rosen, "Optimal needle diameter, shape, and path in autonomous suturing," *ArXiv*, vol. abs/1901.04588, 2019.
- [12] B. Kehoe, G. Kahn, J. Mahler, J.-H. Kim, A. L. A. Lee, K. Nakagawa, S. Patil, W. D. Boyd, P. Abbeel, and K. Goldberg, "Autonomous tumor localization and extraction: Palpation, incision, debridement and adhesive closure with the da Vinci[®] Research Kit," in *Hamlyn Surgical Robotics Conference*, 2015.
- [13] N. Padoy and G. D. Hager, "3D thread tracking for robotic assistance in tele-surgery," in *Proceedings of the IEEE/RSJ International Conference on Intelligent Robots and Systems (IROS 2011)*, 2011, pp. 2102–2017.
- [14] R. C. Jackson, R. Yuan, D. L. Chow, W. S. Newman, and M. C. Cavusoglu, "Real-time visual tracking of dynamic surgical suture threads," *IEEE Transactions on Automation Science and Engineering*, vol. PP, no. 99, pp. 1–13, August 2017.
- [15] O. Ozguner, R. Hao, R. C. Jackson, T. Shkurti, W. Newman, and M. C. Cavusoglu, "Three-dimensional surgical needle localization and tracking using stereo endoscopic image streams," in *IEEE International Conference on Robotics and Automation (ICRA)*, 2018.
- [16] R. Hao, O. Ozguner, and M. C. Cavusoglu, "Vision-based surgical tool pose estimation for the da Vinci robotic surgical system," in *International Conference on Intelligent Robots and Systems (IROS)*, 2018.
- [17] O. Ozguner, T. Shkurti, S. Huang, R. Hao, R. C. Jackson, W. Newman, and M. C. Cavusoglu, "Camera-robot calibration for the da Vinci robotic surgery system," *IEEE Transactions on Automation Science* and Engineering, p. (In Press), 2019, cavusoglu:2018xg.
- [18] C. Staub, T. Osa, A. Knoll, and R. Bauernschmitt, "Automation of tissue piercing using circular needles and vision guidance for computer

- aided laparoscopic surgery," in 2010 IEEE International Conference on Robotics and Automation (ICRA), May 2010, pp. 4585–4590.
- [19] S. Iyer, T. Looi, and J. Drake, "A single arm, single camera system for automated suturing," in 2013 IEEE International Conference on Robotics and Automation, 2013, pp. 239–244.
- [20] A. Shademan, R. S. Decker, J. D. Opfermann, S. Leonard, A. Krieger, and P. C. W. Kim, "Supervised autonomous robotic soft tissue surgery," *Science Translational Medicine*, vol. 8, no. 337, pp. 337ra64–337ra64, 2016. [Online]. Available: https://stm.sciencemag.org/content/8/337/337ra64
- [21] H. Saeidi, H. Le, J. Opfermann, S. Leonard, A. Kim, M. Hsieh, J. U Kang, and A. Krieger, "Autonomous laparoscopic robotic suturing with a novel actuated suturing tool and 3d endoscope," in 2019 IEEE International Conference on Robotics and Automation (ICRA), 05 2019.
- [22] J. Canny, "A computational approach to edge detection," *IEEE Transactions on Pattern Analysis and Machine intelligence*, vol. 6, pp. 679–698, 1986.
- [23] "OpenCV." [Online]. Available: https://opencv.org/
- [24] S. Thrun, W.Burgard, and D. Fox, Probabilistic Robotics. MIT press, 2005.
- [25] P. Kazanzides, Z. Chen, A. Deguet, G. S. Fischer, R. H. Taylor, and S. P. DiMaio, "An open-source research kit for the da Vinci[®] surgical system," in *IEEE International Conference on Robotics and Automation (ICRA)*, 2014.